

# Space Weather®

# بي

### RESEARCH ARTICLE

10.1029/2022SW003321

#### **Key Points:**

- First simultaneous observations of geomagnetic storm effects on equatorial ionization anomaly (EIA) morphology and equatorial plasma bubble (EPB) occurrence rate from the geostationary orbit
- Maximum poleward shift of the EIA crests and increase in EPB occurrence rate is observed during storm's main phase on 27 September 2020
- Concurrent increase of hmF2 from digisonde observation confirms the strengthening of the plasma fountain effect during postsunset hours

#### Correspondence to:

D. K. Karan, Deepak.Karan@lasp.colorado.edu

#### Citation:

Karan, D. K., Eastes, R. W., Daniell, R. E., Martinis, C. R., & McClintock, W. E. (2023). GOLD mission's observation about the geomagnetic storm effects on the nighttime equatorial ionization anomaly (EIA) and equatorial plasma bubbles (EPB) during a solar minimum equinox. *Space Weather*, 21, e2022SW003321. https://doi.org/10.1029/2022SW003321

Received 14 OCT 2022 Accepted 25 JAN 2023

© 2023. The Authors.

This is an open access article under the terms of the Creative Commons Attribution-NonCommercial-NoDerivs License, which permits use and distribution in any medium, provided the original work is properly cited, the use is non-commercial and no modifications or adaptations are made.

## GOLD Mission's Observation About the Geomagnetic Storm Effects on the Nighttime Equatorial Ionization Anomaly (EIA) and Equatorial Plasma Bubbles (EPB) During a Solar Minimum Equinox

Deepak Kumar Karan<sup>1</sup>, Richard W. Eastes<sup>1</sup>, Robert E. Daniell<sup>2</sup>, Carlos R. Martinis<sup>3</sup>, and William E. McClintock<sup>1</sup>

<sup>1</sup>Laboratory for Atmospheric and Space Physics, University of Colorado, Boulder, CO, USA, <sup>2</sup>Ionospheric Physics, Stoughton, MA, USA, <sup>3</sup>Center for Space Physics, Boston University, Boston, MA, USA

**Abstract** The nighttime ionospheric response to a geomagnetic storm that occurred on 23–29 September 2020 is investigated over the South American, Atlantic, and West African longitude sectors using NASA's Global-scale Observations of the Limb and Disk measurements. On 27 September the solar wind conditions were favorable for prompt penetration electric fields to influence the equatorial ionosphere over extended longitudes. The equatorial ionization anomaly (EIA) crests were shifted  $8^{\circ}$ – $10^{\circ}$  poleward compared to the quiet time monthly mean across  $\sim 65^{\circ}$ – $35^{\circ}$ W during the main phase. Ionosonde hmF2 (peak electron density height) measurements from Fortaleza (GG: 3.9°S and 38.4°W) indicated a stronger prereversal enhancement this evening than other nights. As a result, equatorial plasma bubbles (EPB) occurred at these longitudes on this evening. This is the first simultaneous investigation of EIA morphology and EPB occurrence rate over an extended longitude range from geostationary orbit during a geomagnetic storm.

Plain Language Summary The effects of a geomagnetic storm that occurred during 23–29 September 2020 on the nighttime equatorial ionospheric behavior is investigated using NASA's Global-scale Observations of the Limb and Disk (GOLD) measurements. On each evening, the equatorial ionization anomaly (EIA) crests locations and brightnesses and equatorial plasma bubbles (EPB) occurrence rates are obtained over the South American, Atlantic, and West African longitude sectors. On 27 September the solar wind conditions were favorable for the penetration of interplanetary electric fields to the equatorial ionosphere over the dusk longitude sectors (~35°W Lon). The PPEF strengthened the pre-reversal enhancement and thereby enhanced the plasma fountain effect. Ionospheric F2 layer height increase is confirmed by digisonde measurements at Fortaleza (GG: 3.9°S and 38.4°W). On this day, the maximum poleward shifts compared to the quiet time monthly mean values are observed across ~65°–35°W longitude during the storm's main phase. EPBs occurrence rate was maximum on this night. The present study reports the first simultaneous investigation of EIA morphology (crests locations and brightnesses) and EPB occurrence rates over an extended longitude range during a geomagnetic storm from a geostationary orbit.

#### 1. Introduction

The equatorial ionization anomaly (EIA) (also known as the Appleton Anomaly) is a persistent ionospheric feature at equatorial and low latitudes (Appleton, 1946). The equatorial F region eastward electric fields  $(\vec{E})$  and horizontal northward magnetic fields  $(\vec{B})$  create a vertical, upward  $(\vec{E}X\vec{B})$  drift over the magnetic equator. Due to this vertical drift, the ionospheric plasma moves to higher altitudes and diffuses along the magnetic field lines to low latitudes. The overall effect is known as the fountain effect (Hanson & Moffett, 1966; Martyn, 1955). The plasma density shows a minimum at the magnetic equator and two maxima around 15°-20° north and south of it. This creates a double-peaked structure in the latitudinal distribution of the F region plasma with crests on each side and a trough over the magnetic equator, which is called the EIA.

During geomagnetic disturbances, several storm-induced electric fields (e.g., prompt penetration electric field [PPEF], disturbance dynamo electric fields [DDEF]) contribute to the ionospheric electric fields over the equatorial and low latitude regions. During southward conditions of interplanetary magnetic field (IMF) Bz, effects of the Y-component (dawn-dusk) of interplanetary electric field (IEF) can reach equatorial and low latitudes. The

KARAN ET AL.

changes in the equatorial ionospheric electric fields due to the storm time magnetosphere-ionosphere coupling are well understood (Chakrabarty et al., 2008, 2015; Fejer et al., 2008; Rout et al., 2019, and references therein). The resultant electric field can increase or decrease the vertical drift and thereby, can change the strength of the plasma fountain effect and EIA crests locations.

The response of the EIA crests to geomagnetic disturbances using measurements (Aa et al., 2019; Abdu et al., 1991; Akala et al., 2021; Astafyeva, 2009; Balan et al., 2018; Karan & Pallamraju, 2018; Mannucci et al., 2005; Pallamraju et al., 2004) and simulations (Huba et al., 2005; Lu et al., 2013; Tsurutani et al., 2008) have been reported in the literature. Most of these papers discuss the impact of extreme geomagnetic storms on the daytime EIA crests latitudes and electron densities. There are few studies on the effect of geomagnetic disturbance electric fields on the postsunset/nighttime behavior of EIA crests (Abdu et al., 1991; Balan et al., 2018; Huba et al., 2005; Rout et al., 2019). Most of them investigated the storm time EIA behavior over a narrow longitude range.

Geomagnetic storms not only affect the EIA morphology but also affect the behavior of ionospheric plasma irregularities. Due to the pre-reversal enhancement (PRE) at the magnetic equator, local times shortly after sunset favor the development of ionospheric plasma irregularities. Lower atmospheric waves seed the perturbation for the generation of such irregularities (Aa et al., 2020). The irregularities manifest as equatorial plasma bubbles (EPBs) in airglow ionospheric images. Electric field perturbations during geomagnetic active periods are reported to enhance (Basu et al., 2010; Cherniak & Zakharenkova, 2022; Kil et al., 2016; Patra et al., 2016; Tulasi Ram et al., 2008; Zakharenkova & Cherniak, 2020) and sometimes inhibit (Aarons, 1991; Abdu et al., 1995; Spogli et al., 2016) the irregularities. Using the AE-parameterized Fejer-Scherliess model for disturbance vertical drifts versus storm time and local time, Martinis et al. (2005) were able to summarize these apparently contradictory effects.

In the present study, we have used NASA's Global-scale Observations of the Limb and Disk (GOLD) instrument data to investigate the effects of a CIR-storm that occurred during 23–29 September 2020 on both the postsunset EIA crests locations and brightnesses, and the EPB occurrence rates over the South American, Atlantic, and West African longitude sectors. To the best of our knowledge, this study is the first simultaneous investigation on geomagnetic storm effects on EIA morphology and EPB occurrence rate over an extended longitude range from geostationary orbit. Geomagnetic storms of varying strengths can damage the ground and space-based infrastructures and they are also injurious to human health, engineering, and applications (Pulkkinen et al., 2017). With this regard the present investigation on the effects of a moderate CIR geomagnetic storm simultaneously on the nighttime EIA morphology and EPB occurrence rate will assist space weather community's understanding to develop future forecasting capabilities.

#### 2. Data

GOLD images are the primary data set in this work. The imager was launched on 25 January 2018 and is located in geostationary orbit at 47.5°W. The imager has two identical, independent channels (channel A and B; CHA and CHB hereafter), each has a scan mirror and interchangeable slits. GOLD has the advantage of observing the American, Atlantic, and West African longitudinal regions. This provides a unique opportunity to unambiguously observe the spatial-temporal evolution of various ionospheric-thermospheric features of the Earth during post-sunset periods. The GOLD instrument, observation modes, and data products are discussed in Eastes et al. (2017, 2019, 2020) and McClintock et al. (2020). GOLD makes disk and limb observations, and occultations of the Earth at FUV emission wavelength (~132–162 nm). Only the nighttime partial disk, 135.6 nm is assumed to be 300 km when geolocating the pixels. Nightside partial disk observations use both channels. The observations start at 20:10 UT using CHB only, alternating between northern and southern hemispheres. An image is obtained every 15 min, initially over the African sector, and follows the sunset terminator toward the South American sector. From 23:10 UT both channels make simultaneous observations over the northern and southern hemispheres at nearly the same longitude regions. The observation sequence is explained in detail by Karan et al. (2020).

Solar wind parameters (magnetic field, electric field, plasma flow speed, proton density, plasma temperature, and flow pressure), and geomagnetic indices (SYM-H and ap index) are used to understand the solar wind conditions

KARAN ET AL. 2 of 9

15427390, 2023, 3, Downloaded from https://agupubs. onlinelibrary.wiley.com/doi/10.1029/2022SW003321 by Boston University, Wiley Online Library on [23/06/2023]. See the Terms and Conditions (https://or

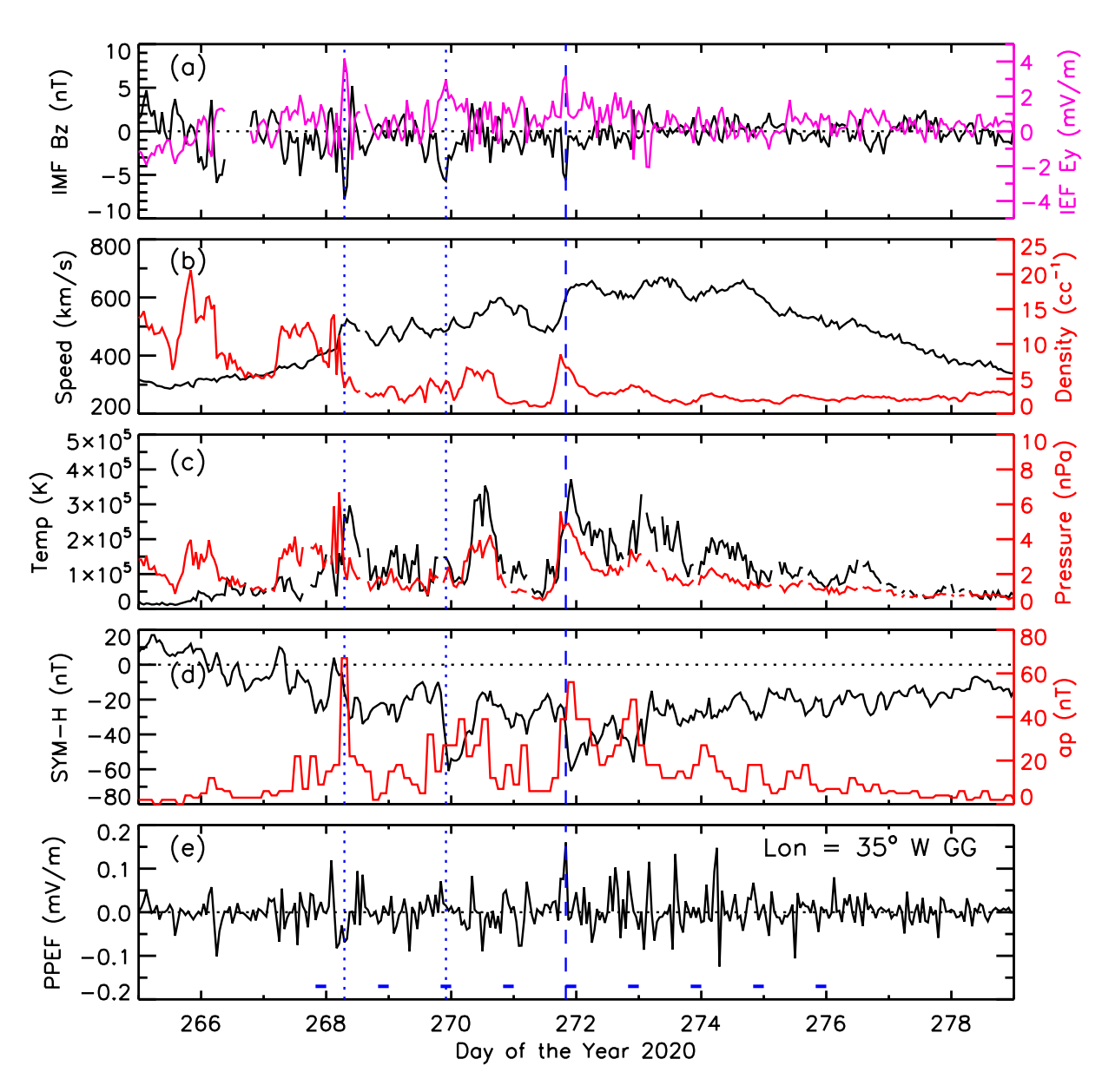


**Figure 1.** (a) Interplanetary magnetic field Bz and interplanetary electric field (IEF) Ey, (b) plasma flow speed and proton density, (c) plasma temperature and flow pressure, (d) SYM-H and ap, and (e) model prompt penetration electric fields during 21 September 2020 (DOY = 265) to 5 October 2020 (DOY = 279).

and different phases of the geomagnetic storm and to evaluate storm's effect on equatorial ionosphere model ionospheric electric fields (Manoj & Maus, 2012). F2 layer height responds to changes in the zonal electric field. So, variations of the ionospheric F2 layer height (hmF2), are obtained from ionosonde observations at Fortaleza (GG: 3.9°S and 38.4°W).

### 3. Results and Discussions

Figures 1a–1c show the hourly averaged solar wind parameters observed at the L1 point from 21 September 2020 (DOY = 265) to 4 October 2020 (DOY = 278). Figure 1d shows the SYM-H and ap indexes derived from ground-based magnetometer measurements. Figure 1e shows modeled ionospheric PPEF obtained from NOAA's Space Weather Prediction Center (https://geomag.colorado.edu/real-time-model-of-the-ionospheric-electric-fields). This PPEF is predicted using a transfer function model using the solar wind data from the Deep Space Climate Observatory (DSCOVR) satellite and NASA/ACE spacecraft (Manoj & Maus, 2012). The horizontal

KARAN ET AL. 3 of 9

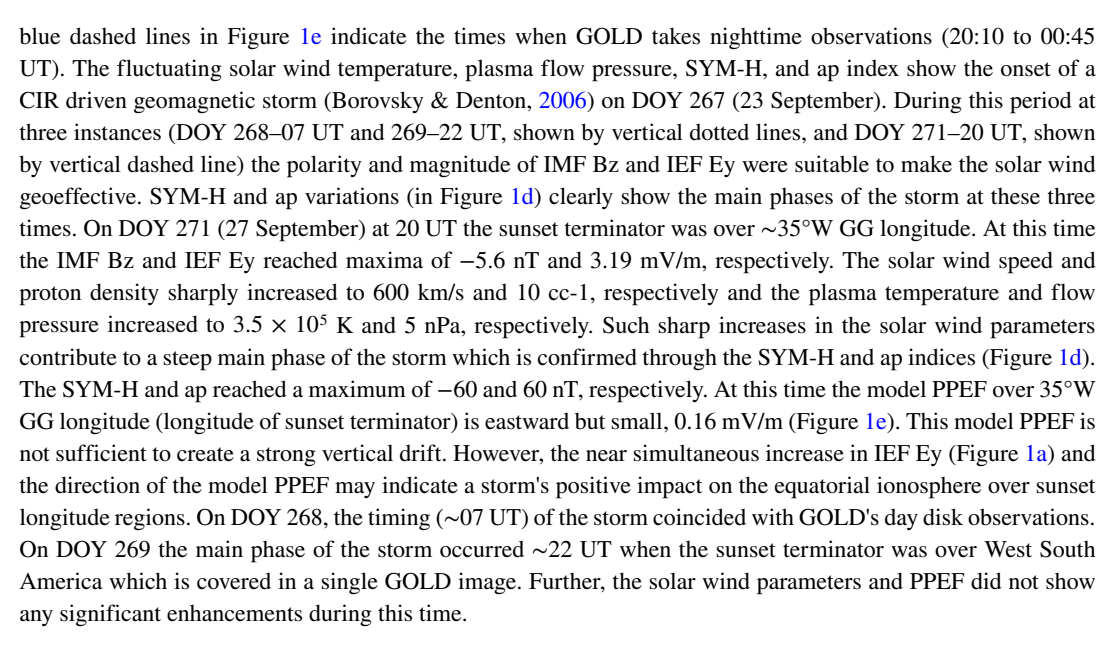
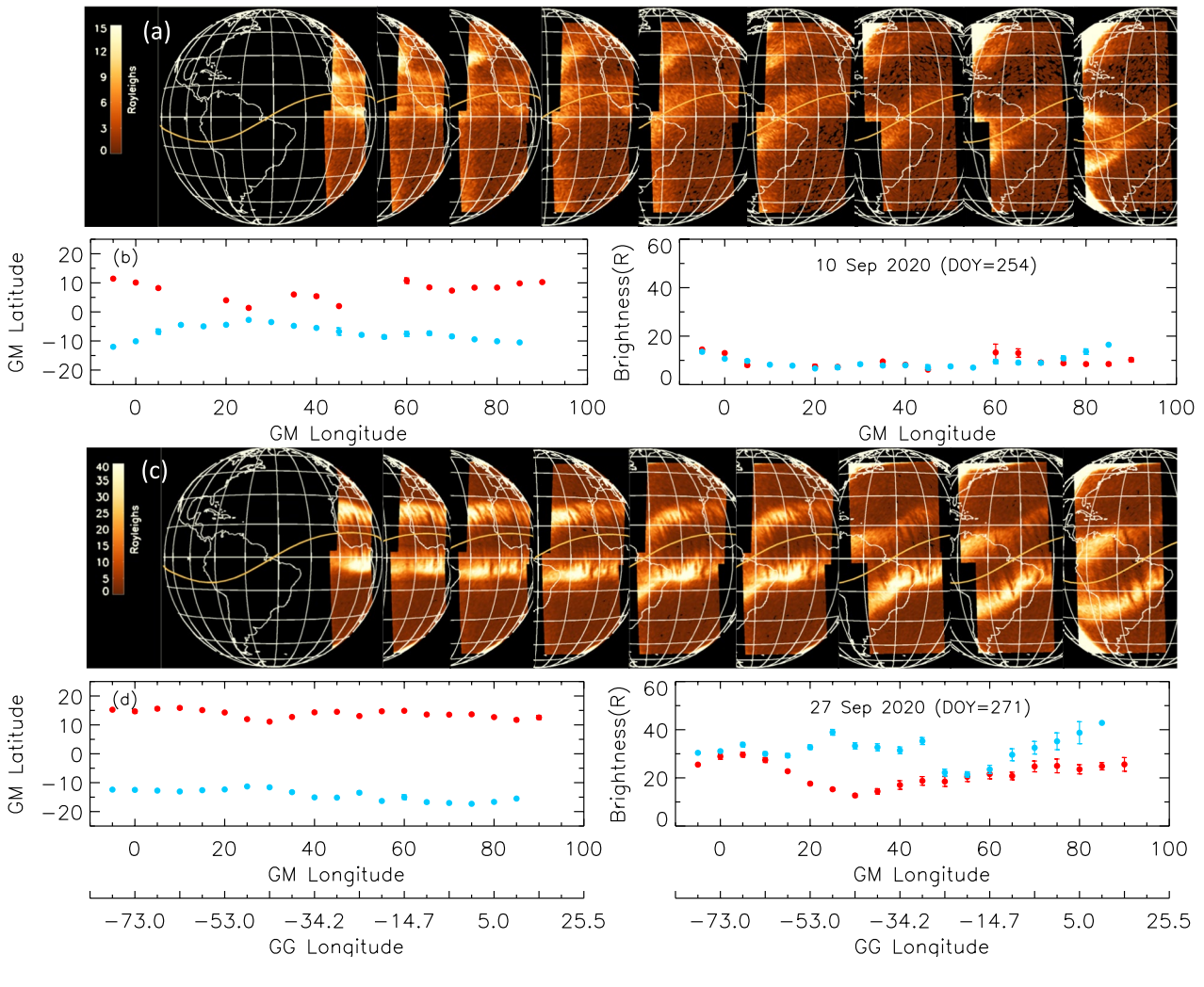


Figure 2a (left to right) shows the composite nightside partial disk images taken by GOLD on DOY 254 (10 September 20:10 to 00:45 UT), a geomagnetic quiet day. As time progresses, the sunset terminator moves westward. So, the longitude coverage of each scan increases (from 23° over West Africa to ~40° over South America). These images are re-mapped into quasi dipole geomagnetic co-ordinates (Laundal & Richmond, 2017) using the International Geomagnetic Reference Field scalar potentials (Thébault et al., 2015). From the remapped images, variations in 135.6 nm brightness with respect to (w.r.t.) magnetic latitudes are obtained at an interval of 1° magnetic longitude. Maxima in the latitudinal variation of the brightness give the location of the EIA crests. Following this method, the EIA crests latitudes and the brightness are obtained from all the images. Sometimes low brightnesses create extraneous EIA crests locations which are filtered out in the analysis which is explained in detail by Eastes et al. (2021). From the filtered values, the average and standard deviation of the North (N) and South (S) crests latitudes and the brightness are obtained every 5° longitude bin. Figure 2b shows the EIA crests latitudes (left) and the brightness (right) (N-red and S-blue) with their standard deviations obtained from the images shown In Figure 2a. The EIA crests locations at 45°-55° magnetic longitudes were not computed due to low signal levels. In Figure 2a the brightness increase at the northern mid latitudes (~30°N) can be seen. An ongoing investigation on this feature is in progress and will be communicated separately. Figures 2c and 2d are similar to Figures 2a and 2b) but for DOY 271 (27 September), a geomagnetic active day. On this day the EIA crests are farther from the magnetic equator and are brighter.

Following the procedure mentioned in the previous paragraph, monthly mean EIA crest latitudes and brightnesses are computed for September 2020, considering quiet days (with ap values less than 20 nT). The relative shifts in the EIA crests latitudes compared to monthly mean values are calculated for the storm days (DOY 268–273). Figures 3a and 3b) show the N and S EIA crests poleward shifts on the storm days. The longitudinal variations of the shifts show similar patterns on these days. This might be indicating a similar systematic longitudinal variation of the electric fields on these days. Figures 3c and 3d) show the brightness of the N and S EIA crests. On these days, in general, the EIA crests brightnesses are higher over West African and South American longitude sectors than the Atlantic longitudes. On DOY 271 the shifts of both crests were consistently greater than on the other nights. A maximum shift of  $\sim$ 8°–10° is observed over  $\sim$ 10°–40° GM Lon ( $\sim$ 65°–35°W GG Lon). Both EIA crests over this longitude sector are brighter on DOY 271. Over  $\sim$ 35°W GG longitude, the S EIA crest is brighter than the N EIA crest by  $\sim$ 20 R.

In order to study the effects of this geomagnetic storm on the behavior of ionospheric plasma irregularities, we investigated EPB occurrences for the full month. An automated tool (described in Karan et al., 2020) is used to obtain the EPBs longitudes from all the images taken on each night. Figure 4a shows all the EPBs observed by GOLD from 1 September to 7 October 2020 as a function of longitude. On the first 11 days (DOY 245–255) the EPBs occurrence was rare, but later it increases during the storm days. Toward the end of September and the beginning of October (DOY 273–280), geomagnetic activity was quiet and EPBs occurrence was low. The red

KARAN ET AL. 4 of 9



**Figure 2.** (a) The nighttime 135.6 nm images of the Earth taken by Global-scale Observations of the Limb and Disk imager on 10 September 2020, a geomagnetic quiet day (max ap = 4); (b) (left) the North (red dots) and South (blue dots) equatorial ionization anomaly (EIA) crests obtained from all images shown in (a); (b) (right) the 135.6 nm brightness at the EIA crests with corresponding colors as in (b) left. (c and d) are similar to (a and b) but for 27 September 2020, a geomagnetic disturbed day (max ap = 56).

line shows the total number of EPBs and the blue line shows the daily mean ap index during 18 to 00 UT (period close to GOLD observations). It can be seen that EPBs occurrence rate and geomagnetic activity mostly agree with each other. Most EPBs were observed east of ~35° W GG longitude during the quiet days (DOY 245–268). On DOY 269 and DOY 271 (geomagnetically active) EPBs are observed west of 35°W GG longitude where EIA crests poleward shifts were maxima. The possible cause for the increase in the poleward shift of the EIA crest and the EPB occurrence rate could be the strengthening of the equatorial electric field due to PPEF effects. If this is true, then the equatorial F2 layer might have moved to a higher altitude. Ionosonde data from Fortaleza (GG: ~3.9°N and ~38.4°W) are used to investigate the behavior of hmF2, the height of peak electron density (Reinisch & Galkin, 2011). This station was chosen because it is located near the magnetic equator and at a longitude where the maximum EIA shift is observed. The mean and standard deviation of hmF2 values during 18–24 UT for the entire month of September 2020 are shown in Figure 4b. This time interval includes the pre and postsunset hmF2 information. On DOY 271, hmF2 was maximum (~350 km) among all the days.

This maximum hmF2 on DOY 271 can be explained by the time (20 UT) of peak IEF Ey (Figure 1a) and variation of SYM-H index (Figure 1d). To examine the enhancement of the ring current, the rate of decrease of SYM-H (i.e., dSYM-H/dt) is investigated (not shown here). dSYM-H/dt has a maximum negative excursion of -12 nT/30 min at 20 UT. The simultaneity of peak IEF Ey and the sharp decrease in SYM-H at 20 UT suggests that there was

KARAN ET AL. 5 of 9

15427390, 2023, 3, Downloaded from https://agupubs.onlinelibrary.wiley.com/doi/10.1029/2022SW003321 by Boston University, Wiley Online Library on [23/06/2023]. See the Terms and Conditions (https://on

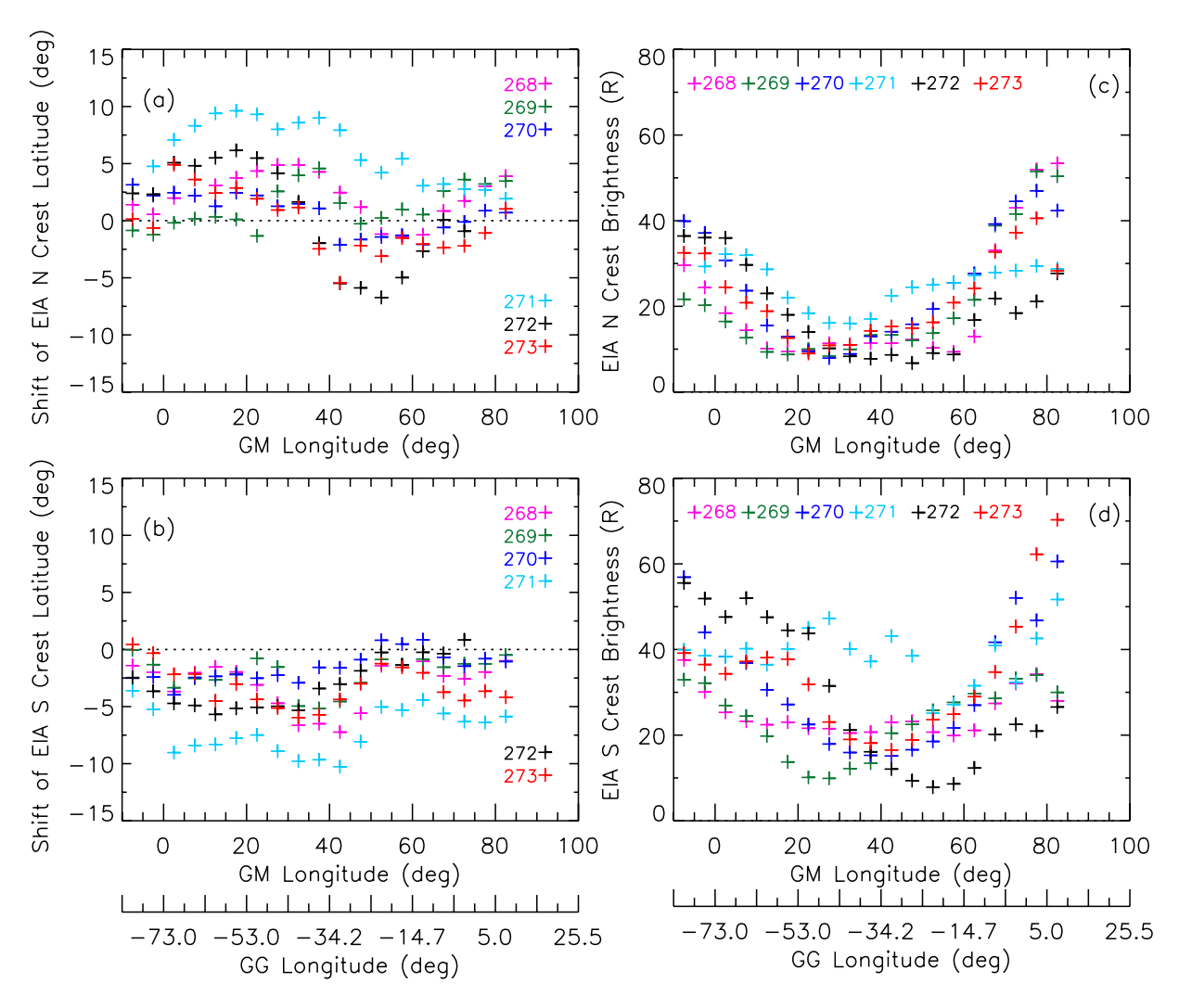


**Figure 3.** The shift of equatorial ionization anomaly (EIA) North (a) and South (b) crests on the disturbed days (DOY 268–273) compared to the geomagnetic quiet days mean value for September 2020. (c and d) The 135.6 nm brightnesses at the North and South EIA crests on the disturbed days.

a prompt penetration of eastward electric fields into the equatorial and low latitudes around local dusk sectors (~35°W GG longitudes). This eastward PPEF increased the normal prereversal enhancement thereby lifting the ionospheric layer up as observed in hmF2 (Figure 4b) and shifting the EIA crests (Figures 3a and 3b). The latitudinal shift of the EIA crests locations was maximum (~8°-10°) over ~10°-40° GM Lon (~65°-35°W GG Lon). These longitudes were in the local sunset hours during the main phase of the storm and thus, were influenced by the PPEF. During major storms, ~12°-15° poleward shifts in the EIA crests were observed (e.g., Mannucci et al., 2005; Rout et al., 2019; Tsurutani et al., 2008). The shifts in the crest latitudes depend on the equatorial electric fields (Karan et al., 2016; Karan & Pallamraju, 2018; Saha & Pallamraju, 2022) that get stronger due to storm induced PPEF. Tulasi Ram et al., 2008 and Basu et al., 2010 have reported the prompt penetration of eastward electric fields into low and equatorial latitudes where the local time corresponds to postsunset hours during the entire main phase of the storm. Their findings match our observations. The shift decreased west of ~65°W GG longitude where local sunset occurred after the main phase. Also, the shifts were less east of ~35°W GG longitude. These longitudes were already in the nightside and had passed through the PRE-process before the main phase of the storm. GOLD's observations over a wide longitudinal coverage have revealed an important understanding of the storm's longitudinal effect.

The lifting of the ionospheric layer to higher altitudes due to strong PRE makes the base of the F layer conducive for RT-instability. This situation is favorable for the occurrence and development of ionospheric plasma irregularities (Abdu et el., 2018; Saha et al., 2022). In the whole month, the highest number of EPBs are observed on the

KARAN ET AL. 6 of 9

15427390, 2023, 3, Downloaded from https://agupubs.onlinelibrary.wiley.com/doi/10.1029/2022SW003321 by Boston University, Wiley Online Library on [23/06/2023]. See the Terms and

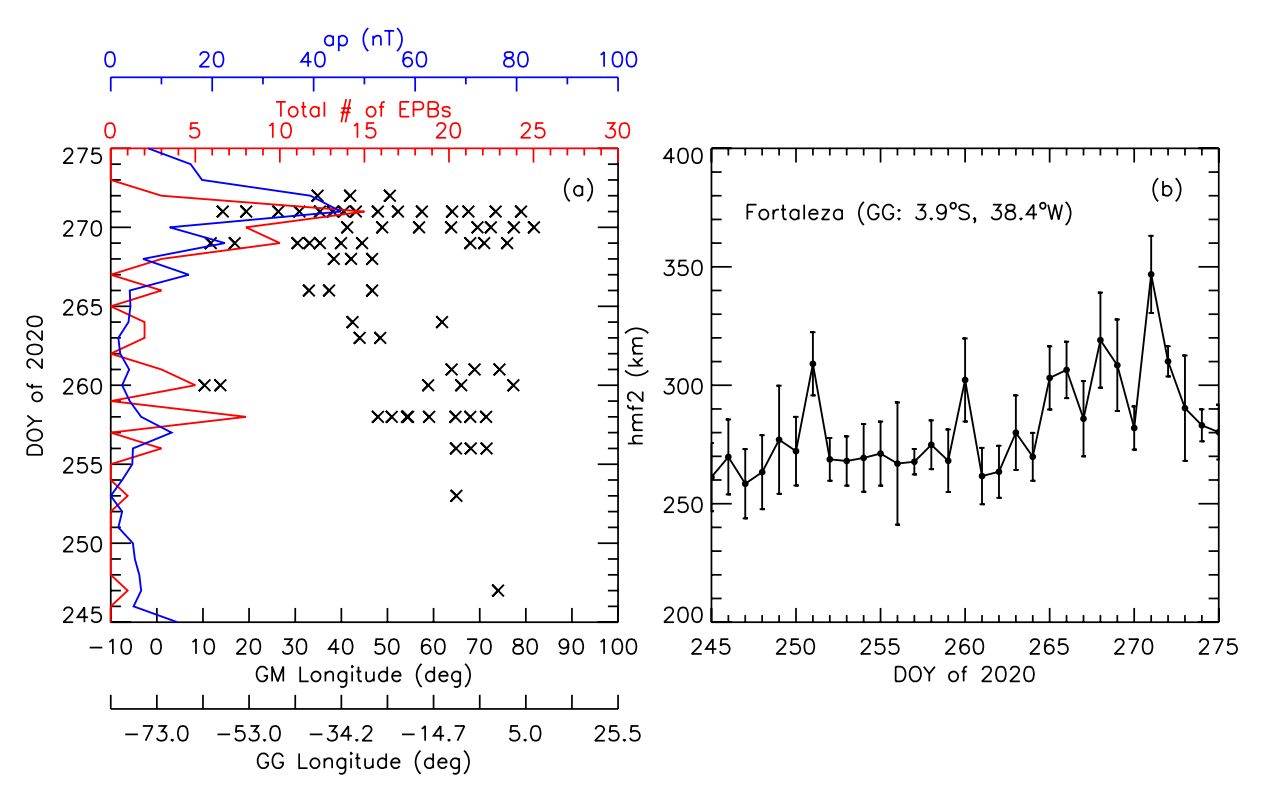


**Figure 4.** (a) Equatorial plasma bubbles (EPB) longitudes (cross symbol) obtained from nighttime images taken by Global-scale Observations of the Limb and Disk imager during September 2020. Day-to-day variations of total EPBs observed (red line) and ap index (blue line) are shown. (b) The hmF2 variation during September 2020 obtained from ionosonde at Fortaleza (GG: 3.9°S and 38.4°W), a geomagnetic equatorial station.

most geomagnetic active day (DOY 271). An Increase in EPBs occurrence rate over  $\sim 10^{\circ}$ – $40^{\circ}$  GM Lon ( $\sim 65^{\circ}$ – $35^{\circ}$ W GG Lon) on the geomagnetic active day indicates the storm's positive effect on EPBs occurrence rate.

#### 4. Conclusions

The present study investigates the effects of a CIR driven geomagnetic storm on the nighttime ionosphere over the South American, Atlantic, and West African longitudes. From GOLD images of the 135.6 nm emission, northern and southern EIA crests latitudes are obtained for all days of September 2020, including the days covering the 23–29 September CIR storm. The EIA crests latitudes during the storm are compared to those before it. While there were significant shifts in the EIA crests locations throughout the storm, the shifts on one night, 27 September, were greater than the others. On that night a maximum shift of  $\sim$ 8°–10° was observed across  $\sim$ 10°–40° GM Lon ( $\sim$ 65°–35°W GG Lon) which correspond to local sunsets during the main phase of the storm. An increase in hmF2 confirms the enhancement of PRE-strength due to storm induced PPEF effect. This favors the development of ionospheric plasma irregularities. EPBs occurrence rate was maximum on DOY 271. The present study reports the first simultaneous investigation of EIA morphology (crests locations and brightnesses) and EPB occurrence rate over an extended longitude range during a geomagnetic storm as observed from geostationary orbit.

### **Data Availability Statement**

The Global-scale Observations of the Limb and Disk (GOLD) data are available from the GOLD Science Data Center (https://gold.cs.ucf.edu/data/search/). The solar wind parameters and geomagnetic indices are taken from the NASA GSFC SPDF OMNI website (https://omniweb.gsfc.nasa.gov/form/omni\_min. html). Model ionospheric electric fields are obtained from (https://geomag.colorado.edu/real-time-model-of-the-ionospheric-electric-fields). Ionosonde data are obtained using the SAO Explorer software obtained from the Global Ionospheric Radio Observatory website (https://ulcar.uml.edu/SAO-X/SAO-X.html and http://spase.info/SMWG/Observatory/GIRO).

KARAN ET AL. 7 of 9

15427390, 2023, 3, Downloaded from https://agupubs

#### Acknowledgments

The principal author thanks Prof. Wenbin Wang for the useful discussions. This research was supported by NASA contract 80GSFC18C0061 to the University of Colorado.

#### References

- Aa, E., Zou, S., Eastes, R., Karan, D. K., Zhang, S.-R., Erickson, P. J., & Coster, A. J. (2020). Coordinated ground-based and space-based observations of equatorial plasma bubbles. *Journal of Geophysical Research: Space Physics*, 125(1), e2019JA027569. https://doi.org/10.1029/2019JA027569
- Aa, E., Zou, S., Ridley, A. J., Zhang, S.-R., Coster, A. J., Erickson, P. J., et al. (2019). Merging of storm time midlatitude traveling ionospheric disturbances and equatorial plasma bubbles. Space Weather, 17(2), 285–298. https://doi.org/10.1029/2018SW002101
- Aarons, J. (1991). The role of the ring current in the generation or inhibition of equatorial F layer irregularities during magnetic storms. *Radio Science*, 26(4), 1131–1149. https://doi.org/10.1029/91RS00473
- Abdu, M. A., Batista, I. S., Walker, G. O., Sobral, J. H. A., Trivedi, N. B., & de Paula, E. R. (1995). Equatorial ionospheric fields during magnetospheric disturbances: Local time/longitudinal dependences from recent EITS Campaigns. *Journal of Atmospheric and Solar-Terrestrial Physics*, 57(10), 1065–1083. https://doi.org/10.1016/0021-9169(94)00123-6
- Abdu, M. A., Nogueira, P. A. B., Santos, A. M., de Souza, J. R., Batista, I. S., & Sobral, J. H. A. (2018). Impact of disturbance electric fields in the evening on prereversal vertical drift and spread F developments in the equatorial ionosphere. *Annales Geophysicae*, 36(2), 609–620. https://doi.org/10.5194/angeo-36-609-2018
- Abdu, M. A., Sobral, J. H. A., de Paula, E. R., & Batista, I. S. (1991). Magnetospheric disturbance effects on the equatorial ionization anomaly (EIA)—An overview. *Journal of Atmospheric and Terrestrial Physics*, 53(8), 757–771. https://doi.org/10.1016/0021-9169(91)90126-R
- Akala, A. O., Oyedokun, O. J., Amaechi, P. O., Simi, K. G., Ogwala, A., & Arowolo, O. A. (2021). Solar origins of August 26, 2018 geomagnetic storm: Responses of the interplanetary medium and equatorial/low-latitude ionosphere to the storm. Space Weather, 19(10), e2021SW002734. https://doi.org/10.1029/2021SW002734
- Appleton, E. (1946). Two anomalies in the ionosphere. Nature, 157(3995), 691. https://doi.org/10.1038/157691a0
- Astafyeva, E. (2009). Effects of strong IMF Bz southward events on the equatorial and mid-latitude ionosphere. *Annales de Geophysique*, 27(3), 1175–1187. https://doi.org/10.5194/angeo-27-1175-2009
- Balan, N., Liu, L. B., & Le, H. J. (2018). A brief review of equatorial ionization anomaly and ionospheric irregularities. Earth and Planetary Physics, 2(4), 257–275. https://doi.org/10.26464/epp2018025
- Basu, S., Basu, S., MacKenzie, E., Bridgwood, C., Valladares, C. E., Groves, K. M., & Carrano, C. (2010). Specification of the occurrence of equatorial ionospheric scintillations during the main phase of large magnetic storms within solar cycle 23. Radio Science, 45(5), RS5009. https://doi.org/10.1029/2009RS004343
- Borovsky, J. E., & Denton, M. H. (2006). Differences between CME-driven storms and CIR-driven storms. *Journal of Geophysical Research*, 111(A7), A07S08. https://doi.org/10.1029/2005JA011447
- Chakrabarty, D., Rout, D., Sekar, R., Narayanan, R., Reeves, G. D., Pant, T. K., et al. (2015). Three different types of electric field disturbances affecting equatorial ionosphere during a long-duration prompt penetration event. *Journal of Geophysical Research: Space Physics*, 120(6), 4993–5008. https://doi.org/10.1002/2014JA020759
- Chakrabarty, D., Sekar, R., Sastri, J. H., & Ravindran, S. (2008). Distinctive effects of interplanetary electric field and substorm on nighttime equatorial F layer: A case study. *Geophysical Research Letters*, 35(19), L19108. https://doi.org/10.1029/2008GL035415
- Cherniak, I., & Zakharenkova, I. (2022). Development of the storm-induced ionospheric irregularities at equatorial and middle latitudes during the 25–26 August 2018 geomagnetic storm. Space Weather, 20, e2021SW002891. https://doi.org/10.1029/2021SW002891
- Eastes, R. W., Karan, D. K., Martinis, C. R., Daniell, R. E., Gan, Q., Burns, A. G., & McClintock, W. E. (2021). GOLD observations of longitudinal variations in the nighttime equatorial ionization anomaly (EIA) crests latitudes. https://doi.org/10.1002/essoar.10506272.1
- Eastes, R. W., McClintock, W. E., Burns, A. G., Anderson, D. N., Andersson, L., Aryal, S., et al. (2020). Initial observations by the Global-scale Observations of the Limb and Disk (GOLD) mission. *Journal of Geophysical Research: Space Physics*, 125(7), e2020JA027823. https://doi.org/10.1029/2020JA027823
- Eastes, R. W., McClintock, W. E., Burns, A. G., Anderson, D. N., Andersson, L., Codrescu, M., et al. (2017). The Global-Scale Observations of the Limb and Disk (GOLD) mission. Space Science Reviews, 212(1–2), 383–408. https://doi.org/10.1007/s11214-017-0392-2
- Eastes, R. W., Solomon, S. C., Daniell, R. E., Anderson, D. N., Burns, A. G., England, S. L., et al. (2019). Global-scale observations of the equatorial ionization anomaly. *Geophysical Research Letters*, 46(16), 9318–9326. https://doi.org/10.1029/2019GL084199
- Fejer, B. G., Jensen, J. W., & Su, S.-Y. (2008). Seasonal and longitudinal dependence of equatorial disturbance vertical plasma drifts. *Geophysical Research Letters*, 35(20), L20106. https://doi.org/10.1029/2008GL035584
- Hanson, W. B., & Moffett, R. J. (1966). Ionization transport effects in the equatorial F region. *Journal of Geophysical Research*, 71(23), 5559–5572. https://doi.org/10.1029/JZ071i023p05559
- Huba, J. D., Joyce, G., Sazykin, S., Wolf, R., & Spiro, R. (2005). Simulation study of penetration electric field effects on the low- to mid-latitude ionosphere. *Geophysical Research Letters*, 32(23), L23101. https://doi.org/10.1029/2005GL024162
- Karan, D. K., Daniell, R. E., England, S. L., Martinis, C. R., Eastes, R. W., Burns, A. G., & McClintock, W. E. (2020). First zonal drift velocity measurement of equatorial plasma bubbles (EPBs) from a geostationary orbit using GOLD data. *Journal of Geophysical Research: Space Physics*, 125(9), e2020JA028173. https://doi.org/10.1029/2020JA028173
- Karan, D. K., & Pallamraju, D. (2018). Effect of geomagnetic storms on the daytime low-latitude thermospheric wave dynamics. *Journal of Atmospheric and Solar-Terrestrial Physics*, 170, 35–47. https://doi.org/10.1016/j.jastp.2018.02.003
- Karan, D. K., Pallamraju, D., Phadke, K. A., Vijayalakshmi, T., Pant, T. K., & Mukherjee, S. (2016). Electrodynamic influence on the diurnal behaviour of neutral daytime airglow emissions. *Annales de Geophysique*, 34(11), 1019–1030. https://doi.org/10.5194/angeo-34-1019-2016
- Kil, H., Lee, W. K., Paxton, L. J., Hairston, M. R., & Jee, G. (2016). Equatorial broad plasma depletions associated with the evening prereversal enhancement and plasma bubbles during the 17 March 2015 storm. *Journal of Geophysical Research: Space Physics*, 121, 10209–10219. https://doi.org/10.1002/2016JA023335
- Laundal, K. M., & Richmond, A. D. (2017). Magnetic coordinate systems. Space Science Reviews, 206(1-4), 27-59. https://doi.org/10.1007/s11214-016-0275-y
- Lu, G., Huba, J. D., & Valladares, C. (2013). Modeling ionospheric super-fountain effect based on the coupled TIMEGCM-SAMI3. Journal of Geophysical Research: Space Physics, 118(5), 2527–2535. https://doi.org/10.1002/jgra.50256
- Mannucci, A. J., Tsurutani, B. T., Iijima, B. A., Komjathy, A., Saito, A., Gonzalez, W. D., et al. (2005). Dayside global ionospheric response to the major interplanetary events of October 29–30, 2003 "Halloween Storms". *Geophysical Research Letters*, 32(12), L12S02. https://doi.org/10.1029/2004GL021467
- Manoj, C., & Maus, S. (2012). A real-time forecast service for the ionospheric equatorial zonal electric field. Space Weather, 10(9), S09002. https://doi.org/10.1029/2012SW000825

KARAN ET AL. 8 of 9



## **Space Weather**

- 10.1029/2022SW003321
- Martinis, C. R., Mendillo, M. J., & Aarons, J. (2005). Toward a synthesis of equatorial spread F onset and suppression during geomagnetic storms. *Journal of Geophysical Research*, 110(A7), A07306. https://doi.org/10.1029/2003JA010362
- Martyn, D. F. (1955). Theory of height and ionization density changes at the maximum of a Chapman-like region, taking account of ion production, decay, diffusion, and total drift. In *Proceedings, Cambridge Conference* (pp. 254–259). Physical Society.
- McClintock, W. E., Eastes, R. W., Beland, S., Bryant, K. B., Burns, A. G., Correira, J., et al. (2020). Global-scale Measurements of the Limb and Disk (GOLD) mission implementation: Observations, data pipeline and level 1 data products. *Journal of Geophysical Research: Space Physics*, 125(5), e2020JA027809. https://doi.org/10.1029/2020JA027809
- Pallamraju, D., Chakrabarti, S., & Valladares, C. E. (2004). Magnetic storm-induced enhancement in neutral composition at low latitudes as inferred by O(1D) dayglow measurements from Chile. *Annales de Geophysique*, 22(9), 3241–3250. https://doi.org/10.5194/angeo-22-3241-2004
- Patra, A. K., Chaitanya, P. P., Dashora, N., Sivakandan, M., & Taori, A. (2016). Highly localized unique electrodynamics and plasma irregularities linked with the 17 March 2015 severe magnetic storm observed using multitechnique common-volume observations from Gadanki, India. Journal of Geophysical Research: Space Physics, 121, 11518–11527. https://doi.org/10.1002/2016JA023384
- Pulkkinen, A., Bernabeu, E., Thomson, A., Viljanen, A., Pirjola, R., Boteler, D., et al. (2017). Geomagnetically induced currents: Science, engineering, and applications readiness. Space Weather, 15(7), 828–856. https://doi.org/10.1002/2016SW001501
- Reinisch, B. W., & Galkin, I. A. (2011). Global ionospheric radio observatory (GIRO). Earth Planets and Space, 63(4), 377–381. https://doi.org/10.5047/eps.2011.03.001
- Rout, D., Pandey, K., Chakrabarty, D., Sekar, R., & Lu, X. (2019). Significant electric field perturbations in low latitude ionosphere due to the passage of two consecutive ICMEs during 6–8 September 2017. *Journal of Geophysical Research: Space Physics*, 124(11), 9494–9510. https://doi.org/10.1029/2019JA027133
- Saha, S., & Pallamraju, D. (2022). Latitudinal variations in the nocturnal behaviour of OI 630 nm airglow emissions and their relationship with equatorial electrodynamics. *Journal of Atmospheric and Solar-Terrestrial Physics*, 241, 105965. https://doi.org/10.1016/j.jastp.2022.105965
- Saha, S., Pallamraju, D., & Ghodpage, R. N. (2022). Investigations of equatorial plasma bubbles as observed in the OI 630 nm nightglow emissions over off-equatorial and low-latitudinal locations over Indian longitudes. Advances in Space Research, 70(11), 3686–3698. https://doi.org/10.1016/j.asr.2022.08.023
- Spogli, L., Cesaroni, C., Di Mauro, D., Pezzopane, M., Alfonsi, L., Musico, E., et al. (2016). Formation of ionospheric irregularities over Southeast Asia during the 2015 St. Patrick's Day storm. *Journal of Geophysical Research: Space Physics*, 121, 12211–12233. https://doi. org/10.1002/2016JA023222
- Thébault, E., Finlay, C. C., Beggan, C. D., Alken, P., Aubert, J., Barroi, O., et al. (2015). International geomagnetic reference field: The 12th generation. Earth Planets and Space, 67(1), 79. https://doi.org/10.1186/s40623-015-0228-9
- Tsurutani, B. T., Verkhoglyadova, O. P., Mannucci, A. J., Saito, A., Araki, T., Yumoto, K., et al. (2008). Prompt penetration electric fields (PPEFs) and their ionospheric effects during the great magnetic storm of 30–31 October 2003. *Journal of Geophysical Research*, 113(A5), A05311. https://doi.org/10.1029/2007JA012879
- Tulasi Ram, S., Rama Rao, P. V. S., Prasad, D. S. V. V. D., Niranjan, K., Gopi Krishna, S., Sridharan, R., & Ravindran, S. (2008). Local time dependent response of postsunset ESF during geomagnetic storms. *Journal of Geophysical Research*, 113(A7), A07310. https://doi.org/10.1029/2007JA012922
- Zakharenkova, I., & Cherniak, I. (2020). When plasma streams tie up equatorial plasma irregularities with auroral ones. Space Weather, 18(2), e2019SW002375. https://doi.org/10.1029/2019SW002375

KARAN ET AL. 9 of 9